Journal of Applied Mathematics and Computing
https://doi.org/10.1007/s12190-024-02359-y

ORIGINAL RESEARCH

Fractional derivative model in COVID-19 dynamics: application to symptom severity and hospital resource allocation in South Korea

Faishal Farrel Herdicho[1] · Sayooj Aby Jose[2,3] · Anuwat Jirawattanapanit[3] · Taesung Park[2,4]

Received: 15 November 2024 / Revised: 29 November 2024 / Accepted: 29 December 2024

Abstract

COVID-19, caused by SARS-CoV-2, has profoundly affected societies worldwide. The high number of cases, along with its widespread effects on health systems, economies, and daily life, has made COVID-19 a critical subject of study. In addition, the limited capacity of healthcare systems and the surge in COVID-19 cases have placed significant pressure on healthcare management. Focusing on the wide range of symptoms with varying severity, this study categorizes symptoms as mild or severe and develops a mathematical model to describe the spread of COVID-19 while accounting for symptom severity. The model incorporates both integer and fractional derivatives, using the Caputo operator, provides a more accurate representation of disease dynamics by capturing long-term dependencies in time-series data. Key properties of the model are analyzed, including solution boundedness, positivity, and the stability of equilibrium points. The model is applied to South Korea's COVID-19 data from June 1 to September 30, 2022, as training data, and from October 1 to 15, 2022, as testing data. The results show superior accuracy of the fractional model over the integer model, as measured by the Mean Absolute Percentage Error (MAPE). A key finding of this study is that prioritizing treatment for mild cases enhances hospital efficiency due to higher recovery rates, offering an effective strategy for managing patient flow under hospital constraints. This modified model, incorporating a saturated

✉ Sayooj Aby Jose
sayooj@snu.ac.kr

✉ Taesung Park
tspark@stats.snu.ac.kr

1 Department of Mathematics, Faculty of Science and Technology, Universitas Airlangga, Surabaya, Indonesia

2 Department of Statistics, Seoul National University, Seoul 08826, Republic of Korea

3 Department of Mathematics, Faculty of Education, Phuket Rajabhat University, Phuket, Thailand

4 Interdisciplinary Program of Bioinformatics, Seoul National University, Seoul 08826, Republic of Korea

Published online: 08 January 2025

form of hospitalization rates, optimizes COVID-19 patient management by aligning treatment strategies with symptom severity, aiming to improve recovery outcomes while balancing the demands on healthcare systems.

Keywords Caputo fractional · COVID-19 · Hospital capacity · Least-square method · Symptom severity

1 Introduction

The COVID-19 pandemic, which first appeared in Wuhan, Hubei province, China in December 2019, quickly spread throughout the world, becoming a global public health problem. This pandemic has impacted the global population, with over 776 million reported cases and 7 million deaths [1]. The high number of cases, along with the widespread impact on health systems, economies, and daily life, has made COVID-19 a critical subject of study, emphasizing the significance of understanding and addressing the pandemic. In South Korea, the first case of COVID-19 was identified in January 2020 from a traveler from Wuhan, China. The epidemic spread rapidly, especially after a large cluster was detected in the city of Daegu. By the end of February 2020, the number of confirmed cases in South Korea was increasing rapidly, causing widespread concern and requiring immediate action [2]. COVID-19 is an infectious disease caused by the SARS-CoV-2 virus. This virus can spread from an infected person's mouth or nose in small liquid particles when they cough, sneeze, speak, sing or breathe. The virus may cause mild or severe symptoms to affected people during the virus replications in their bodies. Symptoms usually begin within 5 to 6 days after exposure and last within 1 to 14 days. The most common symptoms of COVID-19 infection are fever, chills, and sore throat. In some cases, these symptoms may also be accompanied by a runny nose, tiredness, sore eyes, dizziness, and headache. Mild symptoms of COVID-19 infection are characterized by the absence of shortness of breath or severe breathing problems. However, severe symptoms of COVID-19 infection generally resemble those of a lung infection or pneumonia, characterized by severe shortness of breath that makes it difficult for sufferers to move and speak. If not treated immediately, COVID-19 sufferers with severe symptoms are at high risk of developing dangerous complications, such as respiratory failure, sepsis, thromboembolism, multiorgan failure, and also death due to COVID-19 infection [3]. The COVID-19 pandemic has placed an unprecedented strain on health systems, with rapidly increasing demand for healthcare in hospitals and intensive care units (ICUs) worldwide. As the pandemic escalates, determining the resulting needs for healthcare resources (beds, staff, equipment) has become a key priority for many countries [4]. These challenges highlight the urgent need for enhanced healthcare strategies, with epidemiological studies and resource planning playing an essential role in preventing the collapse of health systems during future surges.

Fractional calculus is a branch of mathematical analysis that generalizes the concept of integration and differentiation to non-integer (fractional) orders. Unlike classical calculus, where differentiation and integration are defined for integer orders, fractional calculus allows for the operation of derivatives and integrals to be extended to

any real or complex number. This provides an excellent instrument for the description of memory and hereditary properties of various materials and processes. This is the main advantage of fractional order model in comparison with classical integer order model, in which such effects are in fact neglected [5]. A key component of fractional calculus is the fractional derivative operator, which represents the derivative of a function to a fractional order. The fractional derivative is typically defined in several ways, each offering different ways to handle the initial conditions and interpret the fractional order. Some examples of fractional derivative operators worth mentioning are: Riemann–Liouville, Grunwald–Letnikov, Caputo, Atangana–Baleanu, Atangana–Baleanu–Caputo and Atangana–Fabrizio. All these approaches are defined by an integral except the second one, which is defined by a series.

The mathematical model is a tool for understanding the dynamics of infectious disease transmission, allowing for the prediction and management of infectious disease. Also, the availability of data on infectious diseases will improve estimates of model parameters, allowing the mathematical model explain the spread of disease in a region using these parameter values. Some of the research work done in the field of mathematical modeling related to the COVID-19 problem applied integer order model [6–10] and fractional order model in their frameworks [11–17]. Furthermore, several researchers have also studied the spread of COVID-19 in the fractional order model, including [18] examine the fractional order model of COVID-19 considering two variants of concern in the disease transmission pathway with the Caputo approach, [19] introduced a mathematical model to understand the dynamics of COVID-19 transmission, incorporating both of integer and fractional order derivatives, [20] develop a fractional mathematical model of COVID-19 considering symptomatic and asymptomatic populations with fractal fractional operator and [21] construct a fractional mathematical model of COVID-19 considering heart attack effected patients with fractal fractional operator.

As extrapolated from the prior exposition, we developed a mathematical model to categorize COVID-19 infections based on mild and severe symptoms within the infected population. Our goal is to evaluate treatment strategies based on the classification of mild and severe patients, enabling more targeted and effective interventions aimed at significantly reducing mortality rates and improving outcomes for COVID-19 patients. The use of integer and fractional orders model is also applied in this study to compare the best order in fitting COVID-19 case data in South Korea. Furthermore, we reconstruct the fractional order model by adding hospital capacity constraints to ensure that the model aligns more closely with real-world conditions and presenting numerical simulations to compare several strategies and determine who should be preferentially admitted based on risk groups due to limited hospital capacity. Although COVID-19 cases have subsided at present, this study is still very important as a source of information to assist policymakers in addressing future pandemics and global health challenges.

2 COVID-19 model formulation

In this section, we describe the COVID-19 transmission by considering the severity of the infection. COVID-19, caused by the SARS-CoV-2 virus, can present varying levels of severity. This research is limited to categorizing symptom severity into two classes: mild and severe, to simplify the analysis and focus on the most critical aspects of patient outcomes. Mild symptoms, such as a dry cough, fever, fatigue, and characterized by the absence of respiratory issues often do not require intensive medical care and may allow individuals to continue their activities, although they can still transmit the virus to others in lower chance. This is because individuals with severe symptoms tend to have a high viral load and a long virus shedding period [22]. In contrast, severe symptoms involve respiratory problems, indicate a more serious infection that requires immediate medical attention. Individuals with severe symptoms are often hospitalized and may experience long-term effects from the disease. Understanding these differences is crucial for prioritizing case management, focusing healthcare resources, and developing effective mitigation strategies. Therefore, understanding the distribution of infection severity is essential in COVID-19 prevention and control strategies. Hence, in this model the human population is categorized into six groups: susceptible human (S), Vaccinated human (V), infected human with mild symptoms (I_m), infected human with severe symptoms (I_s), hospitalized human (H) and recovery human (R).

In the transmission, vaccinated individuals are still at risk of infected COVID-19, but at a lower rate than unvaccinated individuals. They may also become susceptible again once the immunity period from the vaccine has been over. When vaccinated individuals become infected with COVID-19, they will always become a mild infection at the beginning of their infection. In contrast, unvaccinated susceptible individuals who are infected with COVID-19 will be classified as mild or severe infections depending on the symptoms they get. Additionally, in this model we assume that the mild infection individuals are not treated in hospital because the symptoms are still mild and they are not aware that they have COVID-19. Many hospitals in South Korea have quickly implemented systems to protect patients and medical staff, including outdoor triage clinics for patients with fever or respiratory symptoms, as well as pre-emptive isolation wards for pneumonia patients [23], with these protective measures in place, it is assumed that individuals hospitalized cannot transmit the COVID-19 virus because they are in isolation.

Then, the notation and description of parameters in the mathematical model of COVID-19 transmission given in Table 1.

Based on the assumptions and descriptions of the variables and parameters that have been explained previously, the transmission diagram of the model is presented in Fig. 1. The mathematical model of COVID-19 transmission by six-dimensional nonlinear autonomous system of ordinary differential equations is presented as follows.

$$\frac{dS}{dt} = \Lambda + \varsigma V - \lambda S - (\eta + \mu)\, S,$$
$$\frac{dV}{dt} = \eta S - (1 - \tau)\, \lambda V - (\varsigma + \mu)\, V,$$

Table 1 Parameters description

Parameters	Description
Λ	Recruitment rate
η	Vaccination rate
ς	Loss of vaccination antibodies rate
β	Transmission rate
θ	Proportion of susceptible become severe infected
τ	Vaccine efficacy
σ	Modification parameter for decrease on infectiousness for I_m
μ	Natural death rate
μ_c	Death rate due to COVID-19
α	Transition rate from I_m to I_s
ρ	Hospitalization rate
φ	Treatment recovery rate
γ_m	Natural recovery rate for I_m
γ_s	Natural recovery rate for I_s

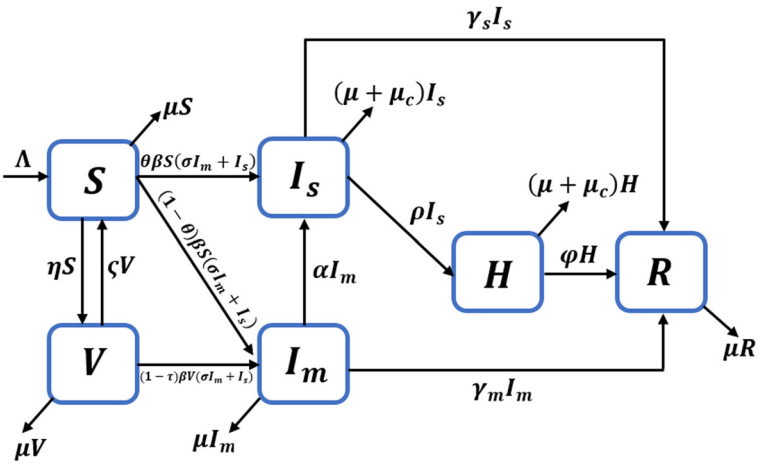

Fig. 1 COVID-19 transmission diagram

$$\begin{aligned}
\frac{dI_m}{dt} &= (1-\theta)\,\lambda S + (1-\tau)\,\lambda V - (\alpha+\gamma_m+\mu)\,I_m,\\
\frac{dI_s}{dt} &= \theta\lambda S + \alpha I_m - (\rho+\gamma_s+\mu_c+\mu)\,I_s,\\
\frac{dH}{dt} &= \rho I_s - (\varphi+\mu_c+\mu)\,H,\\
\frac{dR}{dt} &= \gamma_m I_m + \gamma_s I_s + \varphi H - \mu R.
\end{aligned} \tag{1}$$

with $\lambda = \frac{\beta(\sigma I_m + I_s)}{N}$.

The total human populations is represent by N, where $N = S+V+I_m+I_s+H+R$. Then all parameters in model (1) are assumed to be positive and $0 \leq \theta, \tau, \sigma \leq 1$. The model (1) subject to the initial conditions by $S(0) > 0$, $V(0) \geq 0$, $I_m(0) \geq 0$, $I_s(0) \geq 0$, $H(0) \geq 0$ and $R(0) \geq 0$. Next for simplicity we assume $m_1 = \eta + \mu$, $m_2 = \varsigma + \mu$, $m_3 = \alpha + \gamma_m + \mu$, $m_4 = \rho + \gamma_s + \mu_c + \mu$ and $m_5 = \varphi + \mu_c + \mu$.

3 Positive invariance and boundedness

The solutions of system (1) remain non-negative for all time $t > 0$ and defined in closed set Ω (positively invariant) given as

$$\Omega = \left\{ (S(t), V(t), I_m(t), I_s(t), H(t), R(t)) \in \mathbb{R}^6_+ : N \leq \frac{\Lambda}{\mu} \right\}. \tag{2}$$

Next, we show the positivity solution of system (1) based on the following theorem.

Theorem 3.1 *Let $S(0)$, $V(0)$, $I_m(0)$, $I_s(0)$, $H(0)$, $R(0)$ be the initial conditions of the system (1). If $S(0) \geq 0$, $V(0) \geq 0$, $I_m(0) \geq 0$, $I_s(0) \geq 0$, $H(0) \geq 0$, $R(0) \geq 0$ then all solutions are positive for every $t \geq 0$.*

Proof Take the first equation of the system (1) as follows

$$\begin{aligned}
\frac{dS}{dt} &= \Lambda + \varsigma V - \lambda S - (\eta + \mu) S, \\
\frac{dS}{dt} &\geq -\lambda S - (\eta + \mu) S, \\
\frac{d\left(e^{(\eta+\mu)t + \int_0^t \lambda(s)ds} S(t)\right)}{dt} &\geq 0, \\
S(t) &\geq k e^{-(\eta+\mu)t - \int_0^t \lambda(s)ds},
\end{aligned}$$

with the initial condition $S(0)$ at $t = 0$, we get

$$S(t) \geq S(0)\, e^{-(\eta+\mu)t - \int_0^t \lambda(s)ds}.$$

So $S(t)$ is positive for $t \geq 0$ if $S(0) \geq 0$. Then using the same steps we can prove that $V(t)$, $I_m(t)$, $I_s(t)$, $H(t)$, $R(t)$ also positive for $t \geq 0$. □

4 Model analysis

In this section, we analyze the local and global stability of the equilibrium of model (1). First, we determine the equilibrium with its conditions of existence and the basic reproduction number. From model (1), we obtain two equilibrium, namely the disease-free equilibrium and the endemic equilibrium.

4.1 Disease-free equilibrium point and basic reproduction number

The disease-free equilibrium from model (1) is given by.

$$E_0 = \left(S^0, V^0, I_m^0, I_s^0, H^0, R^0\right) = \left(\frac{\Lambda m_2}{m_1 m_2 - \varsigma\eta}, \frac{\Lambda\eta}{m_1 m_2 - \varsigma\eta}, 0, 0, 0, 0\right).$$

Substitute m_1 and m_2, then with simple calculation we get $m_1 m_2 - \varsigma\eta = \mu\left(\eta + \varsigma + \mu\right)$. So it is clear that S^0 and V^0 are always positive. Then the disease-free equilibrium is always exists.

Next, we determine the basic reproduction number (R_0) that can be used to measure the potential of infection distribution in a population. By using Next Generation Matrix method [24], the matrices F (new infection terms) and V (transition terms) evaluated at the disease-free equilibrium (E_0) are given respectively as follows.

$$F(E_0) = \begin{pmatrix} \frac{(1-\theta)\beta\sigma m_2}{m_2+\eta} + \frac{(1-\tau)\beta\sigma\eta}{m_2+\eta} & \frac{(1-\theta)\beta m_2}{m_2+\eta} + \frac{(1-\tau)\beta\eta}{m_2+\eta} & 0 \\ \frac{\theta\beta\sigma m_2}{m_2+\eta} & \frac{\theta\beta m_2}{m_2+\eta} & 0 \\ 0 & 0 & 0 \end{pmatrix},$$

$$V(E_0) = \begin{pmatrix} m_3 & 0 & 0 \\ -\alpha & m_4 & 0 \\ 0 & -\rho & m_5 \end{pmatrix}.$$

The reproduction number (R_0) is defined by the spectral radius (dominant eigenvalue in magnitude) of the matrix FV^{-1}. Therefore we obtain (R_0) for model (1) is given by.

$$R_0 = \frac{\beta\left(\theta m_2 m_3 + \left(\left(1-\theta\right)m_2 + \left(1-\tau\right)\eta\right)\left(\alpha + \sigma m_4\right)\right)}{m_3 m_4\left(m_2 + \eta\right)}.$$

Next, assuming

$$R_{0s} = \frac{\beta\theta m_2}{m_4\left(m_2+\eta\right)} \text{ and } R_{0m} = \frac{\beta\left(\left(1-\theta\right)m_2 + \left(1-\tau\right)\eta\right)\left(\alpha + \sigma m_4\right)}{m_3 m_4\left(m_2+\eta\right)},$$

we have the equation $R_0 = R_{0s} + R_{0m}$. Furthermore, we can assume again

$$R_{0m1} = \frac{\beta\alpha\left(\left(1-\theta\right)m_2 + \left(1-\tau\right)\eta\right)}{m_3 m_4\left(m_2+\eta\right)} \text{ and } R_{0m2} = \frac{\beta\sigma\left(\left(1-\theta\right)m_2 + \left(1-\tau\right)\eta\right)}{m_3\left(m_2+\eta\right)},$$

as a result $R_{0m} = R_{0m1} + R_{0m2}$, hence

$$R_0 = R_{0s} + R_{0m1} + R_{0m2}. \tag{3}$$

Since all parameters are assumed to be positive, so $R_{0s} < R_0$, $R_{0m1} < R_0$, and $R_{0m2} < R_0$.

4.2 Local stability analysis of disease-free equilibrium point

First, we linearization model (1) as the Jacobian matrix. The Jacobian matrix at E_0 is as following.

$$J(E_0)=\begin{pmatrix} -m_1 & -\varsigma & -\frac{\beta\sigma m_2}{m_2+\eta} & -\frac{\beta m_2}{m_2+\eta} & -0 & 0 \\ \eta & -m_2 & -\frac{(1-\tau)\beta\sigma\eta}{m_2+\eta} & -\frac{(1-\tau)\beta\eta}{m_2+\eta} & 0 & 0 \\ 0 & 0 & \frac{(1-\theta)\beta\sigma m_2}{m_2+\eta}+\frac{(1-\tau)\beta\sigma\eta}{m_2+\eta}-m_3 & \frac{(1-\theta)\beta m_2}{m_2+\eta}+\frac{(1-\tau)\beta\eta}{m_2+\eta} & 0 & 0 \\ 0 & 0 & \frac{\theta\beta\sigma m_2}{m_2+\eta}+\alpha & \frac{\theta\beta m_2}{m_2+\eta}-m_4 & 0 & 0 \\ 0 & 0 & 0 & \rho & -m_5 & 0 \\ 0 & 0 & \gamma_m & \gamma_s & \varphi & -\mu \end{pmatrix}.$$

From the matrix $J(E_0)$, we will look for the characteristic equation with $\det(\lambda I - J(E_0))= 0$, so we get.

$$(\lambda+\mu)(\lambda+m_5)\left(\lambda^2+a_1\lambda+a_2\right)\left(\lambda^2+b_1\lambda+b_2\right)=0, \tag{4}$$

with

$$\begin{aligned} a_1 &= m_1+m_2, \\ a_2 &= m_1m_2+\eta\varsigma, \\ b_1 &= m_3\left[1-R_{0m2}\right]+m_4\left[1-R_{0s}\right], \\ b_2 &= m_3m_4\left[1-R_0\right], \end{aligned}$$

From (4) obtained eigenvalues $\lambda_1 = -\mu$, $\lambda_2 = -m_5$ and the reminders are the roots of the following equation.

$$\lambda^2+a_1\lambda+a_2=0 \text{ and } \lambda^2+b_1\lambda+b_2=0. \tag{5}$$

Since the parameters value are positive, it is clear that $\lambda_1, \lambda_2 < 0$. While using Routh–Hurwitz Criterion, the characteristic equation (5) will have negative real part roots if and only if a_1, a_2, b_1 and $b_2 > 0$. It is clear that coefficient a_1 and a_2 are positive. Coefficient b_1 is positive if $R_{0m2} < 1$ and $R_{0s} < 1$ and coefficient b_2 is positive if $R_0 < 1$. Then, all eigenvalues of matrix $J(E_0)$ are negative if $R_0 < 1$, $R_{0m2} < 1$, and $R_{0s} < 1$. Next based on (3), because $R_{0m2} < R_0$ and $R_{0s} < R_0$, then when $R_0 < 1$ so $R_{0m2} < 1$ and $R_{0s} < 1$ are fulfilled. Therefore, the sufficient and necessary condition for the disease-free equilibrium point is to be locally asymptotically stable if $R_0 < 1$. The foregoing discussion could be summarized in the following theorem.

Theorem 4.1 *The disease-free equilibrium* (E_0) *of the system (1) is locally asymptotically stable if* $R_0 < 1$ *and unstable if* $R_0 > 1$.

4.3 Global stability analysis of disease-free equilibrium point

The global stability of the disease free equilibrium point is investigated using the method described by Castillo-Chavez et al. [25]. Let $X = (S, V, R)^T \in \mathbb{R}^3$ and $Z = (I_m, I_s, H) \in \mathbb{R}^3$, then the model (1) can be rewrite as.

$$\begin{aligned} \frac{dX}{dt} &= F(X, Z), \\ \frac{dZ}{dt} &= G(X, Z), \qquad G(X, 0) = 0. \end{aligned} \tag{6}$$

with $E_0 = (X^0, 0)$ denotes the disease-free equilibrium.

Based on [25] the fixed point $E_0 = (X^0, 0)$ is globally asymptotically stable provided that $R_0 < 1$ and the two conditions bellow are satisfied

$$\begin{aligned} &\text{(H1) For } \frac{dX}{dt} = F(X, 0), X^0 \text{ is globally asymptotically stable.} \\ &\text{(H2) } G(X, Z) = AZ - \widehat{G}(X, Z), \widehat{G}(X, Z) \geq 0 \text{ for } (X, Z) \in \Omega, \end{aligned}$$

with $A = D_Z G(X^0, 0)$ is the M-matrix (the off diagonal elements of A are non-negative). From the system (1) we can get form of system (6) as follows.

$$F(X, Z) = \begin{pmatrix} \Lambda + \varsigma V - \frac{\beta S(\sigma I_m + I_s)}{N} - m_1 S \\ \eta S - (1-\tau)\frac{\beta V(\sigma I_m + I_s)}{N} - m_2 V \\ \gamma_m I_m + \gamma_s I_s + \varphi H - \mu R \end{pmatrix},$$

$$G(X, Z) = \begin{pmatrix} (1-\theta)\frac{\beta S(\sigma I_m + I_s)}{N} + (1-\tau)\frac{\beta V(\sigma I_m + I_s)}{N} - m_3 I_m \\ \theta\frac{\beta S(\sigma I_m + I_s)}{N} + \alpha I_m - m_4 I_s \\ \rho I_s - m_5 H \end{pmatrix}.$$

Furthermore

$$A = \begin{pmatrix} \frac{(1-\theta)\beta\sigma S^0}{N^0} + \frac{(1-\tau)\beta\sigma V^0}{N^0} - m_3 & \frac{(1-\theta)\beta S^0}{N^0} + \frac{(1-\tau)\beta V^0}{N^0} & 0 \\ \frac{\theta\beta\sigma S^0}{N^0} + \alpha & \frac{\theta\beta S^0}{N^0} - m_4 & 0 \\ 0 & \rho & -m_5 \end{pmatrix},$$

$$\widehat{G}(X, Z) = \begin{pmatrix} \frac{(1-\theta)\beta(\sigma I_m + I_s)S^0}{N^0}\left(1 - \frac{SN^0}{NS^0}\right) + \frac{(1-\tau)\beta(\sigma I_m + I_s)V^0}{N^0}\left(1 - \frac{VN^0}{NV^0}\right) \\ \frac{\theta\beta(\sigma I_m + I_s)S^0}{N^0}\left(1 - \frac{SN^0}{NS^0}\right) \\ 0 \end{pmatrix},$$

$$F(X, 0) = \begin{pmatrix} \Lambda + \varsigma V - m_1 S \\ \eta S - m_2 V \\ -\mu R \end{pmatrix}.$$

Solving $\frac{dX}{dt} = F(X, 0)$, we get

$$\begin{pmatrix} S(t) \\ V(t) \\ R(t) \end{pmatrix} = \begin{pmatrix} \frac{\Lambda+\varsigma V}{m_1} + \left(S(0) - \frac{\Lambda+\varsigma V(0)}{m_1}\right) e^{-m_1 t} \\ \frac{\eta S}{m_2} + \left(V(0) - \frac{\eta S(0)}{m_2}\right) e^{-m_2 t} \\ R(0)\, e^{-\mu t} \end{pmatrix}, \tag{7}$$

hence from (7), when $t \to \infty$ and some algebra simplification we get

$$\lim_{t\to\infty} \begin{pmatrix} S(t) \\ V(t) \\ R(t) \end{pmatrix} = \begin{pmatrix} \frac{\Lambda m_2}{m_1 m_2 - \varsigma\eta} \\ \frac{\Lambda\eta}{m_1 m_2 - \varsigma\eta} \\ 0 \end{pmatrix} = \begin{pmatrix} S^0 \\ V^0 \\ R^0 \end{pmatrix}. \tag{8}$$

Equation (8) ensuring the global asymptotic stability of the $X^0 = \left(\frac{\Lambda m_2}{m_1 m_2 - \varsigma\eta}, \frac{\Lambda\eta}{m_1 m_2 - \varsigma\eta}, 0\right)$ hence H1 is satisfied.

Next, solving the first and second equations on model (1) we have $\lim_{t\to\infty} S(t) \leq \frac{\Lambda m_2}{m_1 m_2 - \varsigma\eta} = S^0$ and $\lim_{t\to\infty} V(t) \leq \frac{\Lambda\eta}{m_1 m_2 - \varsigma\eta} = V^0$. Then, it is clear that $S \leq S^0$ and $V \leq V^0$. However, to have $\widehat{G}_1(X, Z) \geq 0$, and $\widehat{G}_2(X, Z) \geq 0$ some conditions are required. For example, we could let the total human population be at equilibrium level ($N = \frac{\Lambda}{\mu} = N^0$) and this condition will be achieved when we assume to ignore the death rate due to COVID-19. This ensures that $\left(1 - \frac{SN^0}{NS^0}\right) \Longleftrightarrow \left(1 - \frac{S}{S^0}\right) \geq 0$ and $\left(1 - \frac{VN^0}{NV^0}\right) \Longleftrightarrow \left(1 - \frac{V}{V^0}\right) \geq 0$. Hence H2 is satisfied. Therefore, because two conditions are fulfilled so the free disease equilibrium point is globally asymptotically stable if we assume to ignore the death rate due to COVID-19. The foregoing discussion could be summarized in the following theorem.

Theorem 4.2 *Suppose that in system (1) the death rate due to COVID-19 is ignored* ($\mu_c = 0$). *If* $R_0 < 1$, *then the disease-free equilibrium point is globally asymptotically stable.*

4.4 Endemic equilibrium point

The endemic equilibrium from model (1) is given by.

$$E_1 = \left(S^*, V^*, I_m^*, I_s^*, H^*, R^*\right),$$

with

$$\begin{aligned} S^* &= \frac{\Lambda\left((1-\tau)\lambda^* + m_2\right)}{\left(\lambda^* + m_1\right)\left((1-\tau)\lambda^* + m_2\right) - \varsigma\eta}, \\ V^* &= \frac{\Lambda\eta}{\left(\lambda^* + m_1\right)\left((1-\tau)\lambda^* + m_2\right) - \varsigma\eta}, \\ I_m^* &= \frac{(1-\theta)\lambda^* S^* + (1-\tau)\lambda^* V^*}{m_3}, \end{aligned} \tag{9}$$

$$I_s^* = \frac{\theta\lambda^* S^* + \alpha I_m^*}{m_4},$$
$$H^* = \frac{\rho}{m_5} I_s^*,$$
$$R^* = \frac{\gamma_m I_m^* + \gamma_s I_s^* + \varphi H^*}{\mu},$$

with λ^* is infection force at steady state defined as $\lambda^* = \frac{\beta(\sigma I_m^* + I_s^*)}{N^*}$.

Next, to show the continuation of Theorem 4.2 that the disease-free equilibrium point is globally asymptotically stable, which means that the existence of backward bifurcation will not occur when the death rate due to COVID-19 is zero. We use special case for assume to ignore the death rate due to COVID-19 ($\mu_c = 0$) to evaluate the endemic equilibrium, hence $N^* = \frac{\Lambda}{\mu}$. Then substitute (9) and $N^* = \frac{\Lambda}{\mu}$ into λ^*, we have λ^* satisfying the quadratic equation

$$c_0\lambda^{*2} + c_1\lambda^* + c_2 = 0,$$

with

$$c_0 = m_3 m_4 (1 - \tau),$$
$$c_2 = m_2 m_3 m_4 + m_1 m_3 m_4 (1 - \tau)[1 - R_1],$$
$$c_3 = m_3 m_4 \mu (m_2 + \eta)[1 - R_0],$$
$$R_1 = \frac{\beta\mu(\theta m_3 + (1 - \theta)(\sigma m_4 + \alpha))}{m_1 m_3 m_4}.$$

Next, with some algebra calculation we have

$$R_0 - R_1 = \frac{\beta\left(\theta m_3^2 m_4 \eta\varsigma + (\alpha + \sigma m_4) m_3 m_4 \eta((1 - \theta)\varsigma + (1 - \tau) m_1)\right)}{m_1 m_3^2 m_4^2 (m_2 + \eta)} > 0.$$

The model (1) will have two endemic equilibriums if $c_2 < 0, c_3 > 0$ (i.e. $R_0 < 1$) and $c_2^2 - -4c_1c_3 > 0$. Suppose $a_3 > 0$ (i.e. $R_0 < 1$), because $R_1 < R_0$, so $R_1 < R_0 < 1$. Hence $R_1 < 1 \Longleftrightarrow 1 - R_1 > 0$. Therefore when $c_3 > 0$ then c_2 always positive cause the model never has two endemic equilibrium points and backward bifurcation does not occur in the model when we assume to ignore the death rate due to COVID-19.

The foregoing discussion could be summarized in the following theorem.

Theorem 4.3 *Suppose that in system (1) the death rate due to COVID-19 is ignored* ($\mu_c = 0$). *Then the system (1) has:*

1. *A unique endemic equilibrium that exist in* Ω *if* $c_3 < 0$ *(i.e.* $R_0 > 1$).
2. *A unique endemic equilibrium that exist in* Ω *if* $c_2 < 0$ *and either* $c_3 = 0$ *(i.e.* $R_0 = 1$) *or* $c_2^2 - 4c_1c_3 = 0$.
3. *No endemic equilibrium otherwise.*

5 Preliminaries of Caputo fractional

In this section, some of the basic principles of Caputo fractional operators and related theorem to support the calculation will addresses.

Definition 5.1 [5] The Caputo fractional derivative of order $\kappa > 0$ of a function $f(t)$ with $n-1 < \kappa < n, n \in \mathbb{N}$ is defined as

$$^{C}\mathcal{D}_{t}^{\kappa} f(t) = \frac{1}{\Gamma(n-\kappa)} \int_{0}^{t} \frac{f^{(n)}(\tau)}{(t-\tau)^{\kappa+1-n}} \, d\tau,$$

with $\Gamma(\cdot)$ is the Gamma Function.

The Riemann–Liouville fractional integral is defined as

$$^{C}\mathcal{D}_{t}^{\kappa} f(t) = \frac{1}{\Gamma(\kappa)} \int_{0}^{t} \frac{f(\tau)}{(t-\tau)^{1-\kappa}} \, d\tau.$$

Definition 5.2 [26] The constant x^* is an equilibrium of the Caputo fractional dynamical system given as

$$^{C}\mathcal{D}_{t}^{\kappa} x(t) = f(t, x(t)), \kappa \in (0, 1) \text{ if only if } f(t, x(t)^*) = 0.$$

6 Fractional COVID-19 model

In this section, we addresses the fractional order model of COVID-19 transmission. The Caputo fractional of model (1) is given by the following system of fractional differential equations.

$$\begin{aligned}
^{C}D_{t}^{\kappa} S &= \Lambda^{\kappa} + \varsigma^{\kappa} V - \lambda^{\kappa} S - \left(\eta^{\kappa} + \mu^{\kappa}\right) S, \\
^{C}D_{t}^{\kappa} V &= \eta^{\kappa} S - (1-\tau)\lambda^{\kappa} V - \left(\varsigma^{\kappa} + \mu^{\kappa}\right) V, \\
^{C}D_{t}^{\kappa} I_m &= (1-\theta)\lambda^{\kappa} S + (1-\tau)\lambda^{\kappa} V - \left(\alpha^{\kappa} + \gamma_m^{\kappa} + \mu^{\kappa}\right) I_m, \\
^{C}D_{t}^{\kappa} I_s &= \theta\lambda^{\kappa} S + \alpha^{\kappa} I_m - \left(\rho^{\kappa} + \gamma_s^{\kappa} + \mu_c^{\kappa} + \mu^{\kappa}\right) I_s, \\
^{C}D_{t}^{\kappa} H &= \rho^{\kappa} I_s - \left(\varphi^{\kappa} + \mu_c^{\kappa} + \mu^{\kappa}\right) H, \\
^{C}D_{t}^{\kappa} R &= \gamma_m^{\kappa} I_m + \gamma_s^{\kappa} I_s + \varphi^{\kappa} H - \mu^{\kappa} R.
\end{aligned} \tag{10}$$

with $\lambda^{\kappa} = \frac{\beta^{\kappa}(\sigma I_m + I_s)}{N}$.

In the above, operator $^{C}D^{\kappa}$ denotes Caputo fractional derivative of order $0 < \kappa \leq 1$. Noting that all the model parameters except τ, σ and θ have dimensions $1/t^{\kappa}$, we have raised these parameters to power of κ for dimensional consistency emphaized by [27].

6.1 Qualitative properties of solution

In this section, we examine the mathematical model and biological well-posedness of the fractional order model (10). In essence, we prove that solution of the fractional order model is bounded and remains positive as long as a positive initial condition is given. Furthermore, we prove the existence and uniqueness of the solution to the modified model.

Let $X(t) = (S, V, I_m, I_s, H, R)^T$ and $\mathcal{K}(t, X(t)) = (\phi_i)^T$, $i = 1, 2, ..., 6$ with

$$\begin{aligned}
\phi_1 &= \Lambda^\kappa + \varsigma^\kappa V - \frac{\beta^\kappa (\sigma I_m + I_s)}{N} S - \left(\eta^\kappa + \mu^\kappa\right) S,\\
\phi_2 &= \eta^\kappa S - (1-\tau)\frac{\beta^\kappa (\sigma I_m + I_s)}{N} V - \left(\varsigma^\kappa + \mu^\kappa\right) V,\\
\phi_3 &= (1-\theta)\frac{\beta^\kappa (\sigma I_m + I_s)}{N} S + (1-\tau)\frac{\beta^\kappa (\sigma I_m + I_s)}{N} V - \left(\alpha^\kappa + \gamma_m^\kappa + \mu^\kappa\right) I_m,\\
\phi_4 &= \theta\frac{\beta^\kappa (\sigma I_m + I_s)}{N} S + \alpha^\kappa I_m - \left(\rho^\kappa + \gamma_s^\kappa + \mu_c^\kappa + \mu^\kappa\right) I_s,\\
\phi_5 &= \rho^\kappa I_s - \left(\varphi^\kappa + \mu_c^\kappa + \mu^\kappa\right) H,\\
\phi_6 &= \gamma_m^\kappa I_m + \gamma_s^\kappa I_s + \varphi^\kappa H - \mu^\kappa R.
\end{aligned}$$

Then the dynamical system (10) can be written as

$$D_t^\kappa X(t) = \mathcal{K}(t, X(t)), \quad X(0) = X_0 \geq 0, \quad t \in [0, b], \quad 0 < \kappa \leq 0 \tag{11}$$

In equation (11), the condition $X(0) \geq 0$ is to be interpreted component-wise. Problem (11), which is equivalent to fractional order model (10) in turn has integral representation

$$\begin{aligned}
X(t) =& X_0 + \mathcal{J}_{0^+}^\kappa \mathcal{K}(t, X(t))\\
=& X_0 + \frac{1}{\Gamma(\kappa)} \int_0^t (t-\tau)^{\kappa-1} \mathcal{K}(\tau, X(\tau))\, d\tau
\end{aligned}$$

Next, we shall analyze model (10) through the integral representation above. For that purpose, let $\mathcal{E} = C([0, b]; \mathbb{R})$ denote the Banach space of all continuous functions from $[0, b]$ to $\mathbb{R}$ endowed with the norm

$$||X||_{\mathcal{E}} = \sup_{t \in [0,b]} \{|X(t)|\}$$

with $|X(t)| = |S(t)| + |V(t)| + |I_m(t)| + |I_s(t)| + |H(t)| + |R(t)|$. Note that S, V, I_m, I_s, H, R all belong to $C([0, b]; \mathbb{R})$. Furthermore, we define the operator $P : \mathcal{E} \to \mathcal{E}$ by

$$(PX)(t) = X_0 + \frac{1}{\Gamma(\kappa)} \int_0^t (t-\tau)^{\kappa-1} \mathcal{K}(\tau, X(\tau))\, d\tau. \tag{12}$$

Note that operator P is well-defined due to obvious continuity of $\mathcal{K}$.

6.1.1 Positivity and boundedness of solution

For the fractional order model (10), its solution is expected to be positive and bounded at all times. These properties are established in the sequel.

Theorem 6.1 *Let $X(t) = (S, V, I_m, I_s, H, R)^T$. Then for $X(0) > 0$, the solution $X(t)$ of model (10) is bounded and remains positive for $t \geq 0$.*

Proof We start by establishing positiveness of solution. Consider the trajectory of solution along the S-axis where $V(0) = I_m(0) = I_s(0) = H(0) = R(0)$ and $S(0) = S_0 > 0$. Then ${}^C D_t^\kappa S = \Lambda^\kappa - (\eta^\kappa + \mu^\kappa)S$, $S(0) = S_0$ whose solution is given by $S(t) = S_0 E_\kappa(-(\eta^\kappa + \mu^\kappa)t^\kappa) + \frac{\Lambda^\kappa}{\eta^\kappa+\mu^\kappa}(1 - E_\kappa(-(\eta^\kappa + \mu^\kappa)t^\kappa)) > 0$. Since $V(0) > 0$, $I_m(0) > 0$, $I_s(0) > 0$, $H(0) > 0$, $R(0) > 0$, similar arguments yield

$$
\begin{aligned}
V(t) &= V_0 E_\kappa(-(\varsigma^\kappa + \mu^\kappa)t^\kappa) + \frac{\eta^\kappa S(t)}{\varsigma^\kappa + \mu^\kappa}(1 - E_\kappa(-(\varsigma^\kappa + \mu^\kappa)t^\kappa)) > 0\\
I_m(t) &= I_{m0} E_\kappa(-(\alpha^\kappa + \gamma_m^\kappa + \mu^\kappa)t^\kappa) > 0\\
I_s(t) &= I_{s0} E_\kappa(-(\rho^\kappa + \gamma_s^\kappa + \mu_c^\kappa + \mu^\kappa)t^\kappa) > 0\\
H(t) &= H_0 E_\kappa(-(\varphi^\kappa + \mu_c^\kappa + \mu^\kappa)t^\kappa) > 0\\
R(t) &= R_0 E_\kappa(-\mu^\kappa t^\kappa) > 0
\end{aligned}
$$

showing non-negative invariance of the axes.

Now, since the solution to the model (10) is positive in the $V - I_m - I_s - H - R$ plane, let $t^* > 0$ such that $S(t^*) = 0$, $V(t^*) > 0$, $I_m(t^*) > 0$, $I_s(t^*) > 0$, $H(t^*) > 0$, $R(t^*) > 0$ and $S(t) < S(t^*)$. On this plane,

$$
{}^C D_t^\kappa S(t)\Big|_{t-t^*} = \Lambda^\kappa > 0 \tag{13}
$$

By Caputo fractional mean value theorem, it hold $S(t) - S(t^*) = \frac{1}{\Gamma(\kappa)} {}^C D_t^\kappa(\tau)(t - t^*)^\kappa$, $\tau \in [t^*, t)$. Therefore, using (13), we obtain $S(t) > S(t^*)$, contradicting our earlier assumption for t^*. Thus, any solution $X(t)$ remains positive for all $t \geq 0$. The remaining variables can be treated similarly. Hence, solution $X(t)$ remains positive for all $t \geq 0$.

Finally for boundedness, proceeding as in the integer order case, we obtains

$$
N(t) \leq N_0 E_\kappa(-\mu^\kappa t^\kappa) + \frac{\Lambda^\kappa}{\mu^\kappa}(1 - E_\kappa(-\mu^\kappa t^\kappa)),
$$

and consequently $\limsup_{t\to\infty} N(t) \leq \frac{\Lambda^\kappa}{\mu^\kappa}$. □

6.1.2 Existence of unique and uniformly stable solution

In this section, we establish existence, uniqueness and uniform stability of solutions to (1) through (10). The following preliminary result is in order.

Lemma 1 *Let* $\bar{X} = (\bar{S}, \bar{V}, \bar{I_m}, \bar{I_s}, \bar{H}, \bar{R})^T$. *The function* $\mathcal{K} = (\phi_i)^T$ *defined above satisfies*

$$||\mathcal{K}(t, X(t)) - \mathcal{K}(t, \bar{X}(t))||_{\mathcal{E}} \leq L_{\mathcal{K}}||X - \bar{X}||_{\mathcal{E}}$$

for some $L_{\mathcal{K}} > 0$.

Proof From the first component of $\mathcal{K}$, we observe that

$$\begin{aligned}
&|\phi_1(t, X(t)) - \phi_1(t, \bar{X}(t))| \\
&= \left|\varsigma^{\kappa}(V(t) - \bar{V}(t)) - \beta^{\kappa}\left(\frac{(\sigma I_m(t) + I_s(t))\, S(t)}{N(t)} - \frac{\left(\sigma \bar{I_m}(t) + \bar{I_s}(t)\right)\bar{S}(t)}{\bar{N}(t)}\right) - \left(\eta^{\kappa} + \mu^{\kappa}\right)(S(t) - \bar{S}(t))\right| \\
&\leq \varsigma^{\kappa}\left|V(t) - \bar{V}(t)\right| + \beta^{\kappa}\left|\frac{(\sigma I_m(t) + I_s(t))\, S(t)}{N(t)} - \frac{\left(\sigma \bar{I_m}(t) + \bar{I_s}(t)\right)\bar{S}(t)}{\bar{N}(t)}\right| + \left(\eta^{\kappa} + \mu^{\kappa}\right)\left|S(t) - \bar{S}(t)\right|
\end{aligned}$$

However,

$$\begin{aligned}
&\left|\frac{(\sigma I_m(t) + I_s(t))\, S(t)}{N(t)} - \frac{\left(\sigma \bar{I_m}(t) + \bar{I_s}(t)\right)\bar{S}(t)}{\bar{N}(t)}\right| \\
&= \left|\frac{(\sigma I_m(t) + I_s(t))\, S(t)\bar{N}(t) - \left(\sigma \bar{I_m}(t) + \bar{I_s}(t)\right)\bar{S}(t)N(t)}{\bar{N}(t)N(t)}\right| \\
&\leq f_1(t)|S(t) - \bar{S}(t)| + f_2(t)|I_m(t) - \bar{I_m}(t)| \\
&\quad + f_3(t)|I_s(t) - \bar{I_s}(t)| + f_4(t)|N(t) - \bar{N}(t)|
\end{aligned}$$

with

$$\begin{aligned}
f_1(t) = \sigma|I_m(t)||\bar{N}(t)| + |I_s(t)||\bar{N}(t)|, \quad f_2(t) = \sigma|\bar{S}(t)||N(t)|, \\
f_3(t) = |\bar{S}(t)||N(t)|, \quad f_4(t) = -\sigma|\bar{S}(t)||I_m(t)| - |\bar{S}(t)||I_s(t)|.
\end{aligned}$$

Note that $f_4(t)$ is negative and this will make Lemma 1 unsatisfied. therefore $f_4(t)|N(t) - \bar{N}(t)|$ must be eliminated, one way is to impose a special case when $N(t) = \bar{N}(t)$ or the total population is constant at all the time. Suppose this condition happens, then we have

$$\begin{aligned}
&\left|\frac{(\sigma I_m(t) + I_s(t))\, S(t)}{N(t)} - \frac{\left(\sigma \bar{I_m}(t) + \bar{I_s}(t)\right)\bar{S}(t)}{\bar{N}(t)}\right| \\
&\leq f_1(t)|S(t) - \bar{S}(t)| + f_2(t)|I_m(t) - \bar{I_m}(t)| + f_3(t)|I_s(t) - \bar{I_s}(t)|
\end{aligned}$$

Altogether, we have

$$\begin{aligned}|\phi_1(t, X(t)) - \phi_1(t, \bar{X}(t))| &\leq (\eta^\kappa + \mu^\kappa + \beta^\kappa f_1(t))|S(t) - \bar{S}(t)| + \varsigma^\kappa |V(t) - \bar{V}(t)| \\ &+ \beta^\kappa f_2(t)|I_m(t) - \bar{I_m}(t)| + \beta^\kappa f_3(t)|I_s(t) - \bar{I_s}(t)| \\ &\leq L_1 \left(|S(t) - \bar{S}(t)| + |V(t) - \bar{V}(t)| + |I_m(t) - \bar{I_m}(t)| + |I_s(t) - \bar{I_s}(t)|\right)\end{aligned}$$

with $L_1 = \eta^\kappa + \mu^\kappa + \varsigma^\kappa + \max\limits_{t\in[0,b]}\{\beta^\kappa f_1(t) + \beta^\kappa f_2(t) + \beta^\kappa f_3(t)\}$.

Similarly we obtain,

$$\begin{aligned}|\phi_2(t, X(t)) - \phi_2(t, \bar{X}(t))| \leq \eta^\kappa |S(t) - \bar{S}(t)| + (\varsigma^\kappa + \mu^\kappa + \beta^\kappa g_1(t))|V(t) - \bar{V}(t)| \\ + \beta^\kappa g_2(t)|I_m(t) - \bar{I_m}(t)| + \beta^\kappa g_3(t)|I_s(t) - \bar{I_s}(t)|\end{aligned}$$

with

$$\begin{aligned}g_1(t) = (1-\tau)\sigma|I_m(t)||\bar{N}(t)| + (1-\tau)|I_s(t)||\bar{N}(t)|, \\ g_2(t) = (1-\tau)\sigma|\bar{V}(t)||N(t)|, \quad g_3(t) = (1-\tau)|\bar{V}(t)||N(t)|.\end{aligned}$$

Hence

$$\begin{aligned}|\phi_2(t, X(t)) - \phi_2(t, \bar{X}(t))| \leq L_2 \left(|S(t) - \bar{S}(t)| + |V(t) - \bar{V}(t)|\right. \\ \left. + |I_m(t) - \bar{I_m}(t)| + |I_s(t) - \bar{I_s}(t)|\right)\end{aligned}$$

with $L_2 = \eta^\kappa + \mu^\kappa + \varsigma^\kappa + \max\limits_{t\in[0,b]}\{\beta^\kappa g_1(t) + \beta^\kappa g_2(t) + \beta^\kappa g_3(t)\}$.

$$\begin{aligned}|\phi_3(t, X(t)) - \phi_3(t, \bar{X}(t))| &\leq (1-\theta)\beta^\kappa f_1(t)|S(t) - \bar{S}(t)| + \beta^\kappa g_1(t)|V(t) - \bar{V}(t)| \\ &+ ((1-\theta)\beta^\kappa f_2(t) + \beta^\kappa g_2(t) + \alpha^\kappa + \gamma_m^\kappa + \mu^\kappa)|I_m(t) - \bar{I_m}(t)| \\ &+ ((1-\theta)\beta^\kappa f_3(t) + \beta^\kappa g_3(t))|I_s(t) - \bar{I_s}(t)| \\ &\leq L_3 \left(|S(t) - \bar{S}(t)| + |V(t) - \bar{V}(t)| + |I_m(t) - \bar{I_m}(t)| + |I_s(t) - \bar{I_s}(t)|\right)\end{aligned}$$

with $L_3 = \alpha^\kappa + \gamma_m^\kappa + \mu^\kappa + \max\limits_{t\in[0,b]}\{(1-\theta)\beta^\kappa(f_1(t) + f_2(t) + f_3(t)) + \beta^\kappa(g_1(t) + g_2(t) + g_3(t))\}$.

$$\begin{aligned}|\phi_4(t, X(t)) - \phi_4(t, \bar{X}(t))| &\leq \theta\beta^\kappa f_1(t)|S(t) - \bar{S}(t)| + (\theta\beta^\kappa f_2(t) + \alpha^\kappa)|I_m(t) - \bar{I_m}(t)| \\ &+ (\theta\beta^\kappa f_3(t) + \rho^\kappa + \gamma_s^\kappa + \mu_c^\kappa + \mu^\kappa)|I_s(t) - \bar{I_s}(t)| \\ &\leq L_4 \left(|S(t) - \bar{S}(t)| + |I_m(t) - \bar{I_m}(t)| + |I_s(t) - \bar{I_s}(t)|\right)\end{aligned}$$

with $L_4 = \alpha^\kappa + \rho^\kappa + \gamma_s^\kappa + \mu_c^\kappa + \mu^\kappa + \max\limits_{t\in[0,b]}\{\theta\beta^\kappa(f_1(t) + f_2(t) + f_3(t))\}$.

For the remaining components of $\mathcal{K}$, it holds

$$\begin{aligned}|\phi_5(t, X(t)) - \phi_5(t, \bar{X}(t))| \leq L_5 \left(|I_s(t) - \bar{I_s}(t)| + |H(t) - \bar{H}(t)|\right) \\ |\phi_6(t, X(t)) - \phi_6(t, \bar{X}(t))| \leq L_6 \left(|I_m(t) - \bar{I_m}(t)| + |I_s(t) - \bar{I_s}(t)|\right.\end{aligned}$$

$$+|H(t)-\bar{H}(t)|+|R(t)-\bar{R}(t)|\big)$$

with $L_5=\rho^\kappa+\varphi^\kappa+\mu_c^\kappa+\mu^\kappa$ and $L_6=\gamma_m^\kappa+\gamma_s^\kappa+\varphi^\kappa+\mu^\kappa$.
Consequently,

$$\begin{aligned}||\mathcal{K}(t,X(t))-\mathcal{K}(t,\bar{X}(t))||_{\mathcal{E}} &= \sup_{t\in[0,b]}\sum_{i=1}^{6}|\phi_i(t,X(t))-\phi_i(t,\bar{X}(t))|\\ &\leq L_{\mathcal{K}}||X-\bar{X}||_{\mathcal{E}}\end{aligned}$$

with $L_{\mathcal{K}}=L_1+L_2+L_3+L_4+L_5+L_6$. Hence Lemma 1 has been proven for special case. □

Theorem 6.2 *Let the result of Lemma 1 holds and* $\Omega=\frac{\Lambda^v}{\Gamma(v+1)}$. *If* $\Omega L_{\mathcal{K}}<1$, *then there exists a unique solution of model (10) on [0,b] which is uniformly Lyapunov stable.*

Proof The function $\mathcal{K}:[0,b]\times\mathbb{R}\to\mathbb{R}_+$ is clearly continuous in its domain. Next, we shall use Banach contraction mapping principle on operator P defined in (12). For that purpose, we show that P is both a self map and a contraction. Firstly, by definition, $\sup_{t\in[0,b]}||\mathcal{K}(t,0)||=\Lambda^v$. Let us now define $\vartheta>\frac{||X_0||+\Omega\Lambda^v}{1-\Omega L_{\mathcal{K}}}$ and a closed convex set $B_\vartheta=\{X\in\mathcal{E}:||X||_{\mathcal{E}}\leq\vartheta\}$. Thus for self map property, it suffices to show that $PB_\vartheta\subseteq B_\vartheta$. Let $X\in B_\vartheta$, then

$$\begin{aligned}||PX||_{\mathcal{E}} &= \sup_{t\in[0,b]}\left\{\left|X_0+\frac{1}{\Gamma(v)}\int_0^t(t-\tau)^{v-1}\mathcal{K}(\tau,X(\tau))\,d\tau\right|\right\}\\ &\leq |X_0|+\frac{1}{\Gamma(v)}\sup_{t\in[0,b]}\left\{\int_0^t(t-\tau)^{v-1}\left(\left|\mathcal{K}(\tau,X(\tau))-\mathcal{K}(\tau,0)\right|+\left|\mathcal{K}(\tau,0)\right|\right)d\tau\right\}\\ &\leq |X_0|+\frac{1}{\Gamma(v)}\sup_{t\in[0,b]}\left\{\int_0^t(t-\tau)^{v-1}\left(\left|\left|\mathcal{K}(\tau,X(\tau))-\mathcal{K}(\tau,0)\right|\right|_{\mathcal{E}}+\left|\left|\mathcal{K}(\tau,0)\right|\right|_{\mathcal{E}}\right)d\tau\right\}\\ &\leq |X_0|+\frac{L_{\mathcal{K}}||X||_{\mathcal{E}}+\Lambda^v}{\Gamma(v)}\sup_{t\in[0,b]}\left\{\int_0^t(t-\tau)^{v-1}\,d\tau\right\}\\ &\leq |X_0|+\frac{L_{\mathcal{K}}\vartheta+\Lambda^v}{\Gamma(v)}\sup_{t\in[0,b]}\left\{\int_0^t(t-\tau)^{v-1}\,d\tau\right\}\\ &= |X_0|+\frac{L_{\mathcal{K}}\vartheta+\Lambda^v}{\Gamma(v+1)}\Lambda^v\\ &= |X_0|+\Omega(L_{\mathcal{K}}\vartheta+\Lambda^v)\\ &\leq \vartheta.\end{aligned}$$

□

It then follows that operator $PX\subseteq B_\vartheta$ and P is indeed a self-map. It remains at this point to prove that P is a contraction. Let X and $\bar{X}\in\mathcal{E}$ satisfy (11). Then again using the result of Lemma 1, we have

$$
\begin{aligned}
||PX - P\bar{X}||_{\mathcal{E}} &= \sup_{t\in[0,b]} \left\{ \left| (PX)(t) - (P\bar{X})(t) \right| \right\} \\
&= \frac{1}{\Gamma(v)} \sup_{t\in[0,b]} \left\{ \int_0^t (t-\tau)^{v-1} \left| \mathcal{K}(\tau, X(\tau)) - \mathcal{K}(\tau, \bar{X}(\tau)) \right| d\tau \right\} \\
&\leq \frac{L_{\mathcal{K}}}{\Gamma(v)} \sup_{t\in[0,b]} \left\{ \int_0^t (t-\tau)^{v-1} \left| X(\tau) - \bar{X}(\tau) \right| d\tau \right\} \\
&\leq \Omega L_{\mathcal{K}} ||X - \bar{X}||_{\mathcal{E}}.
\end{aligned}
$$

Thus if $\Omega L_{\mathcal{K}} < 1$ then P is a contraction mapping, and consequently by the Banach contraction mapping principle, P has a unique fixed point on [0,b] which is solution of (10). Uniformly Lyapunov stability of solution follows from Theorem 3.1.

6.2 Equilibria and basic reproduction number

Using Definition 5.2, the equilibrium points of FDE model (10) are determined by solving the equations
${}^{C}D_t^{\kappa} S(t) = {}^{C}D_t^{\kappa} V(t) = {}^{C}D_t^{\kappa} I_m(t) = {}^{C}D_t^{\kappa} I_s(t) = {}^{C}D_t^{\kappa} H(t) = {}^{C}D_t^{\kappa} R(t) = 0.$
Using some algebra calculation, we obtain equilibrium points same as in model (1) but with different dimension of several parameters, that is $1/t^{\kappa}$.

Basic reproduction number of fractional order model (10) is determined using Next Generation Matrix method [24], first we have consider the system as follows.

$$
{}^{C}D_t^{\kappa} \Omega(t) = F(\Omega(t)) - V(\Omega(t)).
$$

Hence we obtain basic reproduction number same as in model (1) but with different dimension of several parameters, that is $1/t^{\kappa}$.

7 Numerical analysis

In this section, we conduct four numerical analysis. First, parameters estimation on integer and fractional orders model to compare the best order in fitting COVID-19 case data in South Korea in Subsection 7.1. Second, numerical simulation on fractional order model based on the best parameters estimation result in Subsection 7.2. Third, sensitivity Analysis to find the most influential parameters on R_0 in Subsection 7.3. Fourth, simulation the change of β, σ and γ_m as the influence parameters to the population of I_m and I_s in Subsection 7.4.

7.1 Parameters estimation

In this section, we estimate the value of parameter on integer and fractional orders model. First, we collect data from [28], which is daily active cases in South Korea on June 01, 2022– September 30, 2022 as data training and October 01–15, 2022 as data

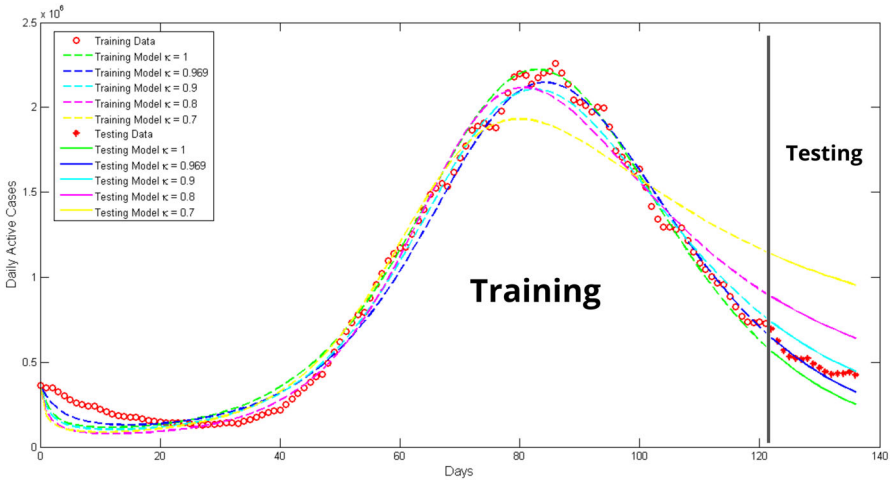

Fig. 2 Parameters estimation result

testing. The selection of this period, which is the second highest wave, is relevant to the mitigation efforts following the first highest wave. Analyzing this wave is important as it provides insights into the effectiveness of public health strategies and adaptation to new variants. In parameter estimation, we use the least-squares method except for parameter λ, μ, and μ_c are obtained from demographic data [28, 29]. The natural death rate is obtained from inverse from the average of life expectancy, so we have $\mu = 0.000033$ per year. Next, for the growth rate of human is obtained from the multiplying the total population by the natural death, hence we have $\Lambda = 1709$ population per year. Furthermore, for death rate due to COVID-19 we approach it with Case Fatality Rate (CFR) that is obtained from the proportion of all individuals who die from COVID-19 among all active cases, so we have $\mu_c = 0.000036$ per year.

The remaining of the parameters in model (1) and (10) is estimated with the goal is to minimize the objective function.

$$\min_{\eta,\beta,\theta,\tau,\sigma,\alpha,\rho,\varphi,\gamma_m,\gamma_s,\varsigma,\kappa} \sum_{i=0}^{t_f} \left(\left(I_{m_i} + I_{s_i} \right) - Data_i \right)^2 ,$$

where t_f is the end time of the daily active cases data $Data_i$ $\left(i = 0, 1, 2, \ldots, t_f\right)$, as well I_{m_i} $\left(i = 0, 1, 2, \ldots, t_f\right)$ and I_{s_i} $\left(i = 0, 1, 2, \ldots, t_f\right)$ are the numerical solutions of mild infection and severe infection population respectively. Next from [28, 29] and some assumption, we set the initial populations such as $\left(S_0; V_0; I_{m_0}; I_{s_0}; H_0; R_0\right) = (51,362,809;\ 59,700;\ 62,767;\ 300,000;\ 1,000;\ 29,532)$. The overall estimation results between the parameter values and order indicate that $\kappa = 0.969$ is the best order in the program's output. Next, we will re-estimate by estimating only the parameter values for several orders that is $\alpha = 0.7, 0.8, 0.9$ and 1, in order to compare the results with the best output. The result of estimation and parameters value can be seen in Fig. 2 and Table 2.

Table 2 Estimated parameters value

κ (fractional order)	0.7 (FDE)	0.8 (FDE)	0.9 (FDE)	0.969 (FDE)	1 (ODE)
Λ	1709	1709	1709	1709	1709
μ	0.000033	0.000033	0.000033	0.000033	0.000033
μ_c	0.000036	0.000036	0.000036	0.000036	0.000036
η	0.057	0.053	0.038	0.028	0.034
ς	0.002	0.002	0.006	0.001	0.007
β	0.888	0.712	0.600	0.535	0.497
θ	0.999	0.984	0.847	0.891	0.784
τ	0.001	0.002	0.001	0.001	0.001
σ	0.991	0.878	0.724	0.649	0.611
α	0.219	0.156	0.086	0.050	0.037
ρ	0.999	0.746	0.613	0.405	0.489
φ	0.360	0.522	0.678	0.775	0.615
γ_m	0.219	0.216	0.180	0.178	0.156
γ_s	0.999	0.747	0.614	0.405	0.489

As shown in Fig. 2, we present a graph showing the number of infected individuals over time, illustrating how the disease spreads biologically with different derivative orders. The fractional-order model reveals a slower or faster decline in infections, depending on delayed interventions or the development of natural immunity. By using fractional derivatives, this model is able to more accurately capture the complex dynamics, highlighting how memory effects and past events influence the current trajectory of the disease. When κ is smaller, the simulation results show a slower decline in infections over time. This can be interpreted as the system remembering the early stages of the outbreak more strongly. Biologically, this is significant because it reflects how past interventions continue to impact the disease dynamics long after the interventions have been implemented.

The best results in this estimation are evaluated using the Mean Absolute Percentage Error (MAPE) with the following formulation.

$$\text{MAPE} = \sum_{i=0}^{t_f} \left| \frac{(I_{m_i} + I_{s_i}) - Data_i}{Data_i} \right| \times 100\%$$

The comparison of errors for training and testing data for each result in Table 2 are presented in the Fig. 3.

Based on Fig. 3, the best fitting data with model solution is indicated by the lowest MAPE value, which is achieved with the fractional order model when $\kappa = 0.969$. Whereas the larger or smaller kappa value compared to 0.969 result in higher errors.

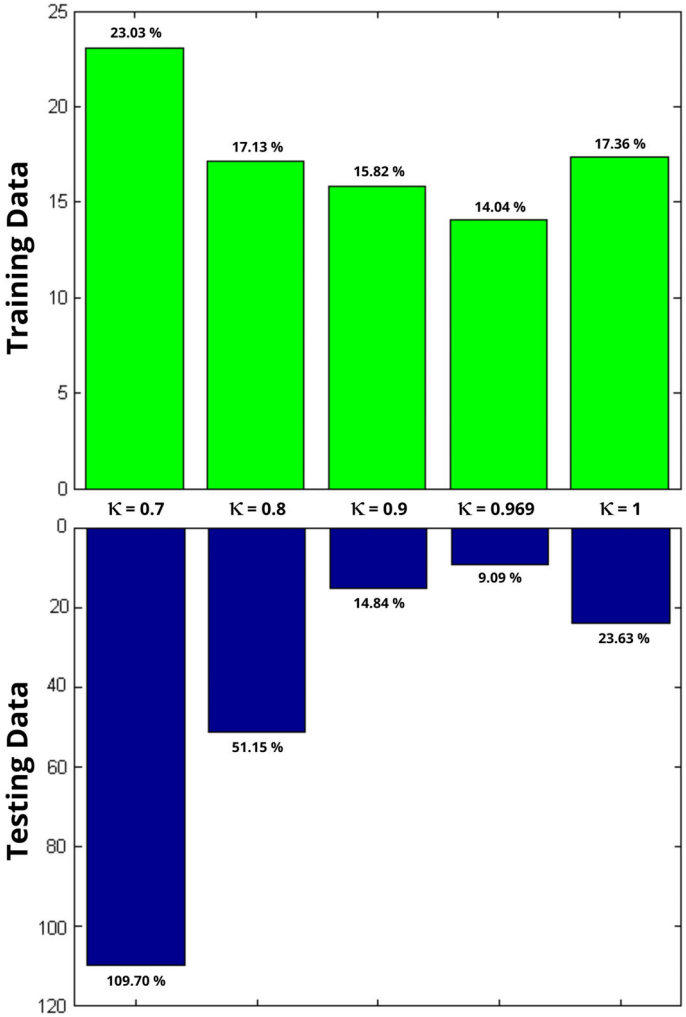

Fig. 3 MAPE comparison for each estimation result

7.2 Simulation of fractional order model

In this section, we simulate the fractional order model 10 using the best parameter estimation results in Table 2 when $\kappa = 0.969$. In this simulation, we set $t_{final} = 150$ days with the results presented in Fig. 4.

Based on Fig. 4b, the population infected with mild symptoms is greater than the population infected with severe symptoms almost all the time, so this needs to be considered in developing a strategy for controlling COVID-19.

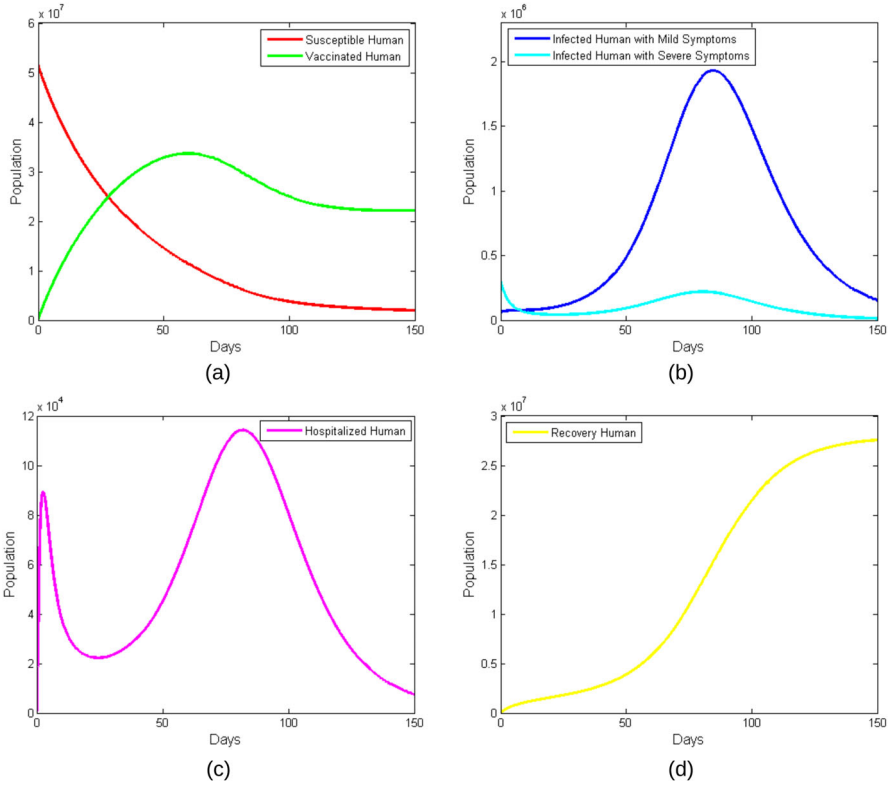

Fig. 4 Numerical simulation on **a** S and V, **b** I_m and I_s, **c** H and **d** R population

7.3 Sensitivity analysis

In this section, we consider the sensitivity analysis to identify the parameter that can impact the basic reproduction number. To determine sensitivity analysis, we followed the technique on [30]. The sensitivity analysis that associate to the parameters is measured by the sensitivity index. The sensitivity index R_0 with respect to a parameter is given by $\Upsilon_a^{R_0} = \frac{\partial R_0}{\partial a} \times \frac{a}{R_0}$. Now we can compute the sensitivity index in Table 3 using parameter value in Table 2 when $\kappa = 0.969$.

Based on Table 3, the positive sign of index shows that when the values of the parameter are raised, the value of R_0 will increase as well. Conversely, the negative sign of index shows that when the value of the parameter are raised, the value of R_0 will decreased. The largest and smallest index from sensitivity index shows the most influential parameters on changes in R_0 are β, σ, and γ_m. Next we simulate the effect of the change of R_0 on two parameters of $\beta - \sigma$ and $\beta - \gamma_m$ in Fig. 5.

Based on contour plot in Fig. 5, it can be seen that the parameter β and σ has a positive relation, however the parameter γ_m has a negative relation, this corresponds to the sign of index sensitivity in Table 3.

Table 3 Sensitivity index of the parameters in R_0

Parameter	Sensitivity Index	Parameter	Sensitivity Index
μ	−0.000744	τ	−0.000984
μ_c	−0.000004	σ	+0.901
η	+ 0.019	α	−0.131
ς	−0.018	ρ	−0.049
β	+ 1	γ_m	−0.771
θ	−0.020	γ_s	−0.049

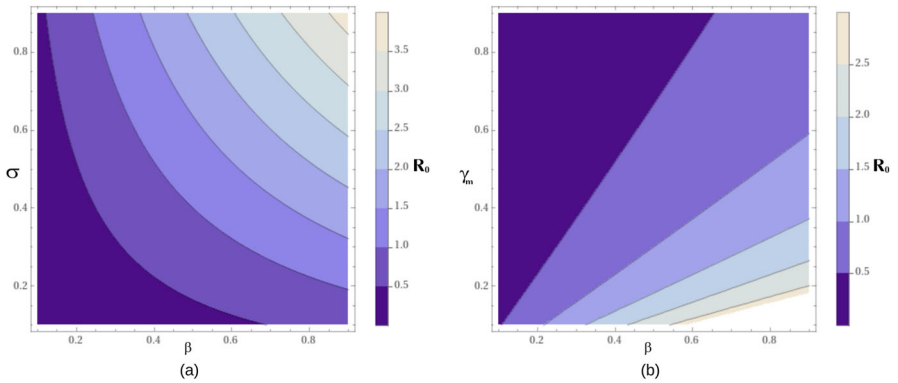

Fig. 5 The effect of the change of R_0 on two parameters of **a** $\beta - \sigma$ and **b** $\beta - \gamma_m$

7.4 Parameters impact

Based on the **Subsection** 7.3, the β, σ and γ_m parameters are the influence parameters. Therefore, in this section, a numerical simulation will be conducted to see the effect of these parameters on the I_m and I_s populations. The results of this simulation is presented in Fig. 6.

The results of the comparison of the cumulative number of infected populations with mild and severe symptoms throughout the simulation time with different parameter values in Fig. 6 are presented in Table 4.

Based on the Table 4, the larger (smaller) the β and σ values result in the number of infected populations with mild and severe symptoms increasing (decreasing). Conversely, the larger (smaller) the γ_m value results in the number of infected populations with mild and severe symptoms decreasing (increasing). Furthermore, based on these three parameters, the most effective way to reduce the number of infected individuals with both mild and severe symptoms is to control the parameter γ_m to be larger, because increasing γ_m by 0.1 can eliminate more infected individuals than decreasing the parameter either β or σ by 0.1.

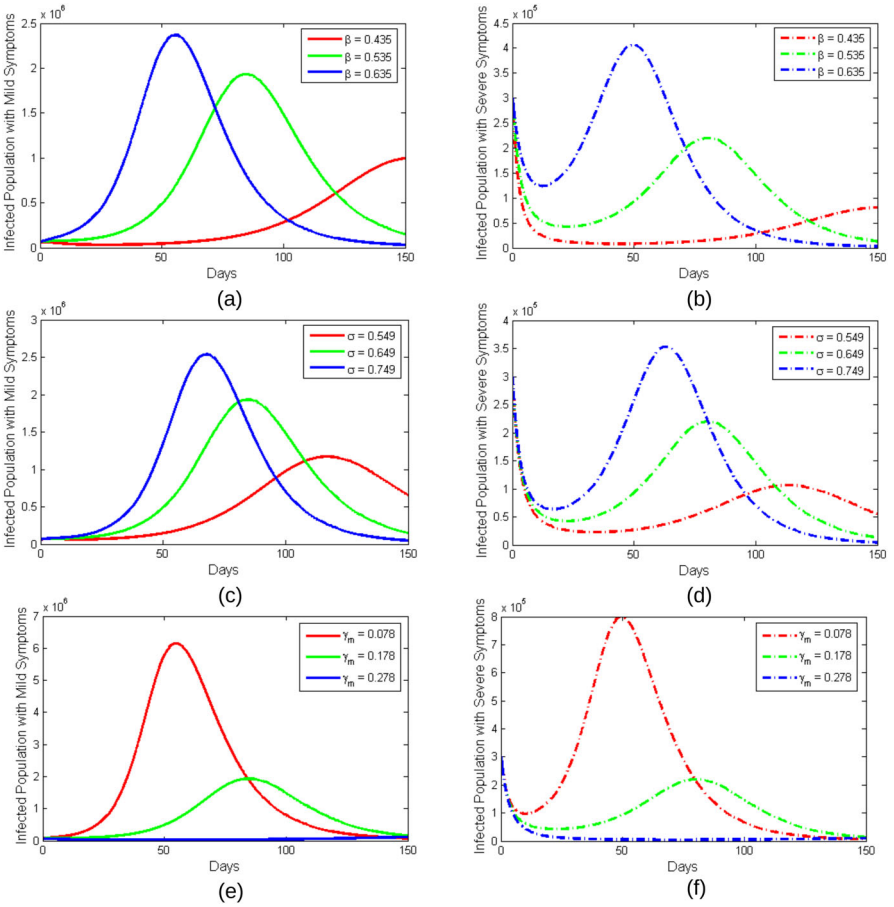

Fig. 6 Impact of parameters on infected populations: (a) β on I_m, (b) β on I_s, (c) σ on I_m, (d) σ on I_s, (e) γ_m on I_m, and (f) γ_m on I_s

Table 4 Numerical simulation result of impact parameters

	Change of β		
	$\beta = 0.435$	$\beta = 0.535$	$\beta = 0.635$
Number of I_m	4.12×10^9	1.11×10^{10}	1.12×10^{10}
Number of I_s	5.03×10^8	1.51×10^9	2.15×10^9
		Change of σ	
	$\sigma = 0.549$	$\sigma = 0.649$	$\sigma = 0.749$
Number of I_m	7.82×10^9	1.11×10^{10}	1.20×10^{10}
Number of I_s	9.59×10^8	1.51×10^9	1.90×10^9
		Change of γ_m	
	$\gamma_m = 0.078$	$\gamma_m = 0.178$	$\gamma_m = 0.278$
Number of I_m	2.63×10^{10}	1.11×10^{10}	6.82×10^8
Number of I_s	3.55×10^9	1.51×10^9	2.28×10^8

8 Hospital Capacity and Infected Patient Flow

Based on Fig. 4c, the number of people being treated in hospital has increased quite high and is not in accordance with the reality of limited hospital capacity. Hence in this section, we reconstruct the model by adding hospital capacity insight in Subsection 8.1 and carrying the simulation for optimizing hospital capacity for COVID-19 management of infected patient flow in Subsection 8.2.

8.1 Mathematical model with hospital capacity

Since in the Subsection 7.1, the fractional order model is better at fitting the COVID-19 spread data in South Korea compared to the integer model, in this section we reconstruct the model 10 by adding hospital capacity insight. This is because the soaring cases of COVID-19 infection have exceeded the hospital's ability to treat patients, so an analysis is needed regarding who should be prioritized for hospitalization for COVID-19 patients between mild or severe symptoms. To capture this phenomenon, the hospitalization rate (ρI) will be changed to a saturated form ($\frac{\rho I}{1+\varrho I}$) to describe a situation in which a hospital capacity reaches the limits of its ability to care for patients so that the infected population being treated will not exceed the hospital capacity availability. The mathematical model with the addition of hospital capacity insight is presented in the following equation

$$
\begin{aligned}
{}^{C}D_t^{\kappa} S &= \Lambda^{\kappa} + \varsigma^{\kappa} V - \lambda^{\kappa} S - \left(\eta^{\kappa} + \mu^{\kappa}\right) S, \\
{}^{C}D_t^{\kappa} V &= \eta^{\kappa} S - (1-\tau)\,\lambda^{\kappa} V - \left(\varsigma^{\kappa} + \mu^{\kappa}\right) V, \\
{}^{C}D_t^{\kappa} I_m &= (1-\theta)\,\lambda^{\kappa} S + (1-\tau)\,\lambda^{\kappa} V - \left(\alpha^{\kappa} + \gamma^{\kappa}{}_m + \mu^{\kappa}\right) I_m - \frac{\rho_m^{\kappa} I_m}{1+\varrho_m I_m}, \\
{}^{C}D_t^{\kappa} I_s &= \theta\lambda^{\kappa} S + \alpha^{\kappa} I_m - \left(\gamma^{\kappa}{}_s + \mu^{\kappa}{}_c + \mu^{\kappa}\right) I_s - \frac{\rho_s^{\kappa} I_s}{1+\varrho_s I_s}, \\
{}^{C}D_t^{\kappa} H &= \frac{\rho_m^{\kappa} I_m}{1+\varrho_m I_m} + \frac{\rho_s^{\kappa} I_s}{1+\varrho_s I_s} - \left(\varphi^{\kappa} + \mu^{\kappa}{}_c + \mu^{\kappa}\right) H, \\
{}^{C}D_t^{\kappa} R &= \gamma^{\kappa}{}_m I_m + \gamma^{\kappa}{}_s I_s + \varphi^{\kappa} H - \mu^{\kappa} R.
\end{aligned}
\tag{14}
$$

with $\lambda^{\kappa} = \frac{\beta^{\kappa}(\sigma I_m + I_s)}{N}$.

8.2 Infected patient flow strategy

In this section, we simulate Model (14) using the best-fitting parameter values in 2 and apply it to several patient flow strategies. First, we look for information about the number of hospital capacities in South Korea, based on [31] the number of hospital bed densities in South Korea in 2021 is 12,770. So we assume a bed density of 10,500 as the hospital capacity for COVID-19 patients. Then, to conduct an analysis of hospital capacity in managing the flow of infected patients, we established 5 strategies.

Table 5 Numerical simulation result

Strategies	Hospital Capacity	Saturation Point	Number of Recovery
1	$I_m = 2,100$	$\varrho_m = 0.000248$	5.84368
(80% I_s) and (20% I_m)	$I_s = 8,400$	$\varrho_s = 0.00006133$	$\times 10^{10}$
2	$I_m = 4,200$	$\varrho_m = 0.0001238$	5.83958
(60% I_s) and (40% I_m)	$I_s = 6,300$	$\varrho_s = 0.00008205$	$\times 10^{10}$
3	$I_m = 5,250$	$\varrho_m = 0.0000989$	5.83915
(50% I_s) and (50% I_m)	$I_s = 5,250$	$\varrho_s = 0.00009861$	$\times 10^{10}$
4	$I_m = 6,300$	$\varrho_m = 0.00008236$	5.84007
(40% I_s) and (60% I_m)	$I_s = 4,200$	$\varrho_s = 0.0001235$	$\times 10^{10}$
5	$I_m = 8,400$	$\varrho_m = 0.00006163$	5.84489
(20% I_s) and (80% I_m)	$I_s = 2,100$	$\varrho_s = 0.0002479$	$\times 10^{10}$

1. **Strategy 1**. In this strategy, hospital capacity is allocated to COVID-19 patients with severe symptoms by 80% of hospital capacity and mild symptoms by 20% of hospital capacity. This strategy is carried out for prioritizes COVID-19 patients with severe symptoms.
2. **Strategy 2**. In this strategy, hospital capacity is allocated to COVID-19 patients with severe symptoms by 60% of hospital capacity and mild symptoms by 40% of hospital capacity. This strategy is carried out so that there is no gap between infected patients but still a slight prioritizes COVID-19 patients with severe symptoms.
3. **Strategy 3**. In this strategy, hospital capacity is allocated to COVID-19 patients with severe symptoms by 50% of hospital capacity and mild symptoms by 50% of hospital capacity. This strategy is carried out so that there is no gap between infected patients with equal proportions.
4. **Strategy 4**.In this strategy, hospital capacity is allocated to COVID-19 patients with severe symptoms by 40% of hospital capacity and mild symptoms by 60% of hospital capacity. This strategy is carried out so that there is no gap between infected patients but still a slight prioritizes COVID-19 patients with mild symptoms.
5. **Strategy 5**. In this strategy, hospital capacity is allocated to COVID-19 patients with severe symptoms by 20% of hospital capacity and mild symptoms by 80% of hospital capacity. This strategy is carried out for prioritizes COVID-19 patients with mild symptoms.

Based on the five strategies, the number of individuals who recovered during the observation period will be evaluated. The best strategy is the strategy that produces the largest number of individuals recovered. In conducting this simulation, we set $t_{final} = 50$ days and the value of $\rho_m = \rho_s = \rho$ which means that the rate of treatment between the mild and severe infected population is not differentiated, but but we differentiate the values of ϱ_m and ϱ_s to ensure that the hospital capacity meets the conditions of each strategy. The results of this simulation is summarized in Table 5 and Figs. 7, 8.

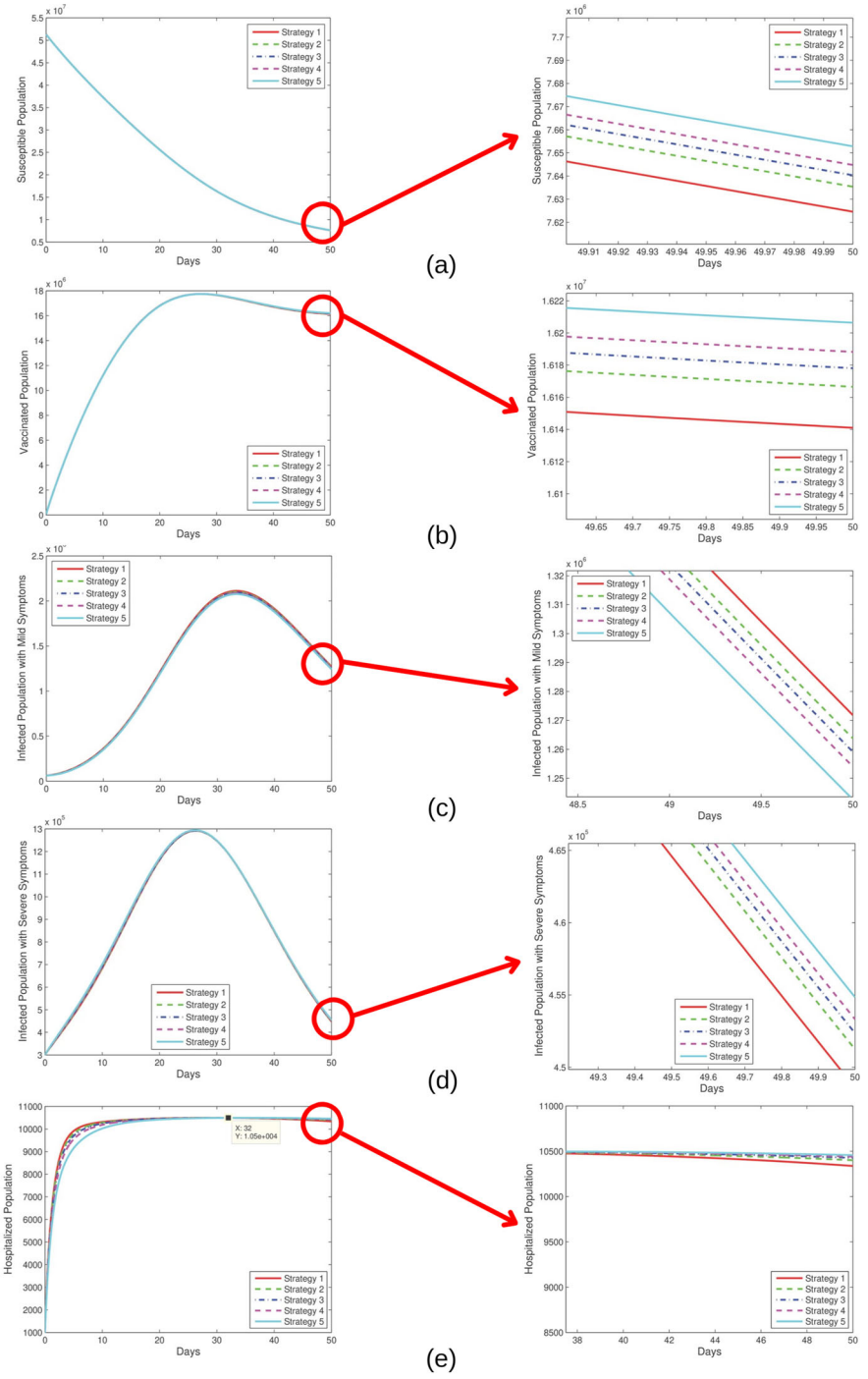

Fig. 7 Numerical simulation of **a** S, **b** V, **c** I_m, **d** I_s and **e** H population

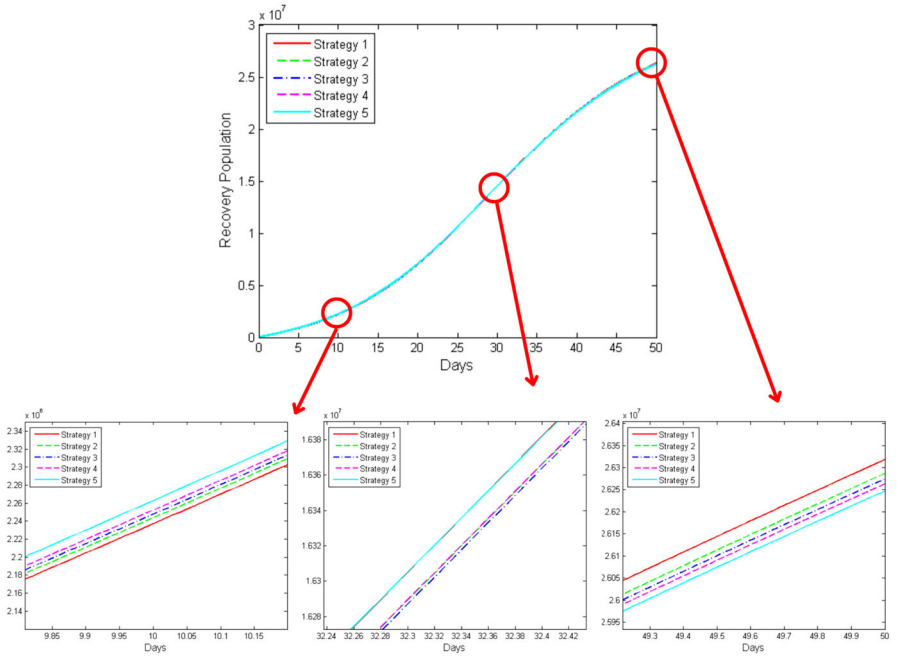

Fig. 8 Numerical simulation of recovery population

Based on Fig. 7e, it is clear that the implementation of hospital capacity has been met as seen from the population treated not exceeding the capacity of 10,500 people. Furthermore, in Fig. 7, the results of the difference in strategies in each population are not very visible because the difference between the number of hospital capacities and the population value is quite far. Therefore, because the focus of the goal is on the recovered population, the zoom detail is only carried out on the recovered population. In Fig. 8, it can be seen that from the beginning to the end of the observation, there is no dominant strategy that always has a high value. Therefore, we evaluate based on the cumulative number of recovery populations from the beginning to the end of the observation in Table 5. Then, we can conclude that implementing Strategy 5 is the best strategy to evaluate the number of recovered populations. This is because the number of mild infected populations is greater compared to severe infected populations. Therefore, early prevention is necessary so that even mild infected populations can be treated early and do not become severe infected population and die.

Conclusion

In this research, we investigate the spread of COVID-19 in South Korea by formulating a mathematical model that combines integer and fractional derivatives order. The purpose of using fractional model is to provide better adjustment and flexibility in interpreting the data. The fractional model allows us to handle long-term dependencies

and complex patterns in time series data, which are difficult to achieve with the integer model. By using the fractional model, we can gain more accurate and in-depth insights into data patterns and trends. This research explores the basic properties of the model: identifying the boundedness, positivity, existence and uniqueness of the solution; analytical analysis; and numerical analysis. The results of the analytical analysis obtained two equilibria: a disease-free equilibrium that is locally and globally asymptotically stable if $R_0 < 1$, and a unique endemic equilibrium that exists if $R_0 > 1$. These results are guaranteed under the assumption of a constant total population, which represents a limitation of this research. The next exploration is to estimate the parameters, we conclude that the model with fractional order, specifically using the Caputo derivative, is better than integer order in fitting the daily active cases data of COVID-19 in South Korea from June 1 to September 30, 2022, as training data, and from October 1 to October 15, 2022, as testing data in terms of Mean Absolute Percentage Error (MAPE). Next based on the sensitivity analysis, the parameters that have the greatest impact on the basic reproduction are transmission rate, modification parameter for decrease on infectiousness for I_m, and natural recovery rate for I_m. Furthermore, based on the simulation of these three parameters, controlling changes in the natural recovery rate for infected human with mild symptoms is the best thing in reducing the infected population because of its most significant influence. The main focus of this research is to optimize treatment pathways for COVID-19 patients based on infection severity and hospital constraints. A reconstruction model has been developed to improve patient flow management and ensure effective resource allocation between mild and severe cases. We suggest that the implementation of hospital treatment of 20% for infected individuals with severe symptoms and 80% percent for infected individuals with mild symptoms is the best strategy to cure patients infected with COVID-19. These findings align with the sensitivity analysis, which suggests that the best strategy for controlling COVID-19 is to prioritize care for individuals with mild infections while ensuring that those with severe infections also receive necessary treatment. Future updates for this research could involve exploring additional fractional operators alongside machine learning and deep learning techniques to enhance model performance. By integrating various fractional calculus approaches with advanced algorithms, we could capture more complex dynamics of COVID-19 spread and improve prediction accuracy. This approach would enable a deeper understanding of the disease's behavior, supporting the development of more effective public health interventions.

Funding This research was supported by grants from the Ministry of Science and ICT, Republic of Korea (No.2021M3E5E3081425) and Phuket Rajabhat University, Thailand.

Declarations

Conflict of interest The authors declare that they have no known competing financial interests or personal relationships that could have appeared to influence the work reported in this paper.

References

1. World Health Organization: WHO COVID-19 dashboard, Available from: (2024). https://data.who.int/dashboards/covid19 [Accessed on November 27th, 2024]
2. Our World in Data: Emerging COVID-19 success story: South Korea learned the lessons of MERS, Available from: (2021). https://ourworldindata.org/covid-exemplar-south-korea [Accessed on August 3rd, 2024]
3. World Health Organization, Coronavirus disease (COVID-19), Available from: (2023). https://www.who.int/news-room/fact-sheets/detail/coronavirus-disease-(covid-19) [Accessed on August 3rd, 2024]
4. Rees, E. M., Nightingale, E. S., Jafari, Y., Waterlow, N. R., Clifford, S., Pearson, C. A. B., Group, C. W., Jombart, T., Procter, S. R. & Knight, G. M.: COVID-19 length of hospital stay: a systematic review and data synthesis. BMC Med. **18**, 270 (2020). https://doi.org/10.1186/s12916-020-01726-3
5. Podlubny, I.: Fractional Differential Equations, Mathematics in Science and Engineering, vol. 198. Academic Press, San Diego, California, USA (1999)
6. Musa, S.S., Qureshi, S., Zhao, S., Yusuf, A., Mustapha, U.T., He, D.: Mathematical modeling of COVID-19 epidemic with effect of awareness programs. Infect. Dis. Modell. **6**(2021), 448–460 (2021). https://doi.org/10.1016/j.idm.2021.01.012
7. Thomas, R., Jose, S.A., Raja, R., Alzabut, J., Cao, J., Balas, V.E.: Modeling and analysis of SEIRS epidemic models using homotopy pertubation method: a special outlook to 2019-nCov in India. Int. J. Biomath. **15**(8), 2250059 (2022). https://doi.org/10.1142/S1793524522500590
8. Chukwu, C.W., Alqahtani, R.T., Alfiniyah, C., Herdicho, F.F.: A Pontryagin's maximum principle and optimal control model with cost-effectiveness analysis of the COVID-19 epidemic. Decis. Anal. J. **8**, 100273 (2023). https://doi.org/10.1016/j.dajour.2023.100273
9. Peter, O.J., Panigoro, H.S., Abidemi, A., Ojo, M.M., Oguntolu, F.A.: Mathematical model of COVID-19 pandemic with double dose vaccination. Acta Biotheoretica **71**(2023), 9 (2023)
10. Rois, M.A., Alfiniyah, C., Martini, S., Aldila, D., Nyabadza, F.: Modeling and optimal control of COVID-19 with comorbidity and three-dose vaccination in Indonesia. J. Biosaf. Biosecur. **6**(3), 181–195 (2024). https://doi.org/10.1016/j.jobb.2024.06.004
11. Jose, S.A., Raja, R., Baleanu, D., Panigoro, H.S., Balas, V.E.: Computational dynamics of a fractional order substance addictions transfer model with Atangana–Baleanu–Caputo derivative. Math. Methods Appl. Sci. **46**(5), 5060–5085 (2022). https://doi.org/10.1002/mma.8818
12. Anggriani, N., Panigoro, H.S., Rahmi, E., Peter, O.J., Jose, S.A.: A Predator–Prey model with additive allee effect and intraspecific competition on predator involving Atangana–Baleanu–Caputo derivative. Res. Phys. **2023**, 106489 (2023). https://doi.org/10.1016/j.rinp.2023.106489
13. Joseph, D., Ramachandran, R., Alzabut, J., Jose, S.A., Khan, H.: Fractional order-density dependent mathematical model to find the better strain of Wolbachia. Symmetry **15**(4), 845 (2023). https://doi.org/10.3390/sym15040845
14. Jose, S.A., Yaagoub, Z., Joseph, D., Ramachandran, R., Jirawattanapanit, A.: Computational dynamics of a fractional order model of chickenpox spread in Phuket province. Biomed. Signal Process. Control **91**, 105994 (2024). https://doi.org/10.1016/j.bspc.2024.105994
15. Ahmad, A., Farman, M., Naik, P.A., Faiz, K., Ghaffar, A., Hincal, E., Saleem, M.U.: Analytical analysis and bifurcation of pine wilt dynamical transmission with host vector and nonlinear incidence using sustainable fractional approach. Partial Differ. Eq. Appl. Math. **11**, 10083 (2024). https://doi.org/10.1016/j.padiff.2024.100830
16. Faiz, K., Ahmad, A., Khan, M.S., Abbas, S.: Control of Marburg Virus Disease Spread in Humans under Hypersensitive Response through Fractal-Fractional. Journal of Mathematical Modeling and Fractional Calculus **1**(1), 88–113 (2024). https://acspublisher.com/journals/index.php/jmmfc/article/view/19860
17. Ahmad, A., Abbas, F., Farman, M., Hincal, E., Ghaffar, A., Akgül, A., Hassani, M.K.: Flip bifurcation analysis and mathematical modeling of cholera disease by taking control measures. Sci. Rep. (2024). https://doi.org/10.1038/s41598-024-59640-0
18. Fatmawati, Yuliani, E., Alfiniyah, C., Juga, M.L., Chukwu, C.W.: On the Modeling of COVID-19 Transmission Dynamics with Two Strains: Insight through Caputo Fractional Derivative, fractal and fractional, **2022**(6), 346 (2022). https://doi.org/10.3390/fractalfract6070346

19. Shamil, E., Jose, S.A., Panigoro, H.S., Jirawattanapanit, A., Omede, B.I., Yaagoub, Z.: Understanding COVID-19 Propagation: a comprehensive mathematical model with Caputo fractional derivatives for Thailand. Front. Appl. Math. Stat. **10**, 1374721 (2024). https://doi.org/10.3389/fams.2024.1374721
20. Ahmad, A., Farooq, Q.M., Ahmad, H., Ozsahin, D.U., Tchier, F., Ghaffar, A., Mustafa, G.: Study on symptomatic and asymptomatic transmissions of COVID-19 including flip bifurcation. Int. J. Biomath. **20**(2024), 699–717 (2024). https://doi.org/10.1142/S1793524524500025
21. Ahmad, A., Abbas, S., Inc, M., Ghaffar, A.: Stability analysis of SARS-CoV-2 with heart attack effected patients and bifurcation. Adv. Biol. **8**(4), 2300540 (2024). https://doi.org/10.1002/adbi.202300540
22. Liu, Y., Yan, L.M., Wan, L., Xiang, T.X., Le, A., Liu, J.M., Peiris, M., Poon, L.L.M., Zhang, W.: Viral dynamics in mild and severe cases of COVID-19. Lancet Infect. Dis. **20**(2020), 656–657 (2020). https://doi.org/10.1016/S1473-3099(20)30232-2
23. Choi, J.Y.: COVID-19 in South Korea. Postgrad. Med. J. **96**(1137), 339–402 (2020). https://doi.org/10.1136/postgradmedj-2020-137738
24. Van den Driessche, P., Watmough, J.: Reproduction numbers and sub-threshold endemic equilibria for compartemental models of disease transmission. Math. Biosci. **180**, 29–48 (2002). https://doi.org/10.1016/S0025-5564(02)00108-6
25. Castillo-Chavez, C., Blower, S., van den Driessche, P., Kirschner, D., Yakubu, A.A.: Mathematical Approaches for Emerging and Reemerging Infectious Diseases. Springer-Verlag, New York (2002)
26. Li, Y., Chen, Y.Q., Podlubny, I.: Stability of fractional-order nonlinear dynamic systems: Lyapunov direct method and generalized Mittag–Leffler stability. Comput. Math. Appl. **59**(2010), 1810–1821 (2010). https://doi.org/10.1016/j.camwa.2009.08.019
27. Diethelm, K.: A fractional calculus based model for the simulation of an outbreak of dengue fever. Nonlinear Dyn. **71**(4), 613–619 (2013). https://doi.org/10.1007/s11071-012-0475-2
28. Worldometers: Worldometer's COVID-19 data in South Korea, Available from: (2024). https://www.worldometers.info/coronavirus/country/south-korea/ [Accessed on June 15th, 2024]
29. Our World in Data: South Korea: Coronavirus Pandemic Country Profile, Available from: (2024). https://ourworldindata.org/coronavirus/country/south-korea [Accessed on June 15th, 2024]
30. Chitnis, N., Hyman, J.M., Cushing, J.M.: Determining important parameters in the spread of malaria through the sensitivity analysis of a mathematical model. Bull. Math. Biol. **70**, 1272–1296 (2008). https://doi.org/10.1007/s11538-008-9299-0
31. Statista: Hospital bed density in South Korea from 2002 to 2021, Available from: (2024). https://www.statista.com/statistics/647213/hospital-bed-density-south-korea/ [Accessed on July 20th, 2024]